

Article

Insights into the Kinetics, Theoretical Model and Mechanism of Free Radical Synergistic Degradation of Micropollutants in UV/Peroxydisulfate Process

Zhixiong Liu ¹, Wenlei Qin ², Lei Sun ¹, Huiyu Dong ², Xiangjuan Yuan ^{1,3,*} , Fei Pan ¹  and Dongsheng Xia ^{1,3,*}¹ School of Environmental Engineering, Wuhan Textile University, Wuhan 430073, China² Research Center for Eco-Environmental Sciences, University of Chinese Academy of Sciences, 18 Shuang-qing Road, Beijing 100085, China³ Engineering Research Center for Clean Production of Textile Dyeing and Printing, Ministry of Education, Wuhan 430073, China

* Correspondence: yuanxiangjuan1986@outlook.com (X.Y.); dongsheng_xia@wtu.edu.cn (D.X.); Tel.: +86-027-5936-7685 (X.Y.); Fax: +86-027-5936-7338 (X.Y.)

Abstract: The degradation of acyclovir (ACY) and atenolol (ATL) in the UV/peroxydisulfate (UV/PDS) process has been systematically considered, focusing on the degradation kinetics, theoretical models, and reaction pathways via applying a microfluidic UV reaction system. The removal efficiencies of ACY and ATL were >94.8%, and the apparent degradation rate constants (k_{obs}) were 0.0931 and 0.1938 min⁻¹ at pH 6.0 in the UV/PDS system. The sulfate radical (SO₄^{•-}) and hydroxyl radical (•OH) were identified as the major reactive radicals. The pH-dependent reaction rate constants of ACY and ATL with •OH and SO₄^{•-} were measured via the competing kinetics. Meanwhile, the contributions of •OH and SO₄^{•-} for ACY and ATL degradation were calculated by the radical steady-state hypothesis, and the results revealed that SO₄^{•-} occupied a decisive position (>84.5%) for the elimination of ACY and ATL. The contribution of •OH became more significant with the increasing pH, while SO₄^{•-} was still dominant. Moreover, ACY and ATL degradation performance were systematically evaluated via the experiments and Kintecus model under different operational parameters (Cl⁻, Br⁻, HCO₃⁻, NOM, etc.) in the UV/PDS process. Furthermore, the plausible reaction pathways of ACY and ATL were elucidated based on the Fukui function theory and ultra-performance liquid chromatography-tandem quadrupole time-of-flight mass spectrometry (UPLC-QTOF-MS) analysis. The UV/PDS process has been demonstrated to be an efficient and potential application for micropollutants mitigation.

Keywords: UV/PDS; micropollutants; radical contribution rates; kinetic models; degradation pathways

Citation: Liu, Z.; Qin, W.; Sun, L.; Dong, H.; Yuan, X.; Pan, F.; Xia, D. Insights into the Kinetics, Theoretical Model and Mechanism of Free Radical Synergistic Degradation of Micropollutants in UV/Peroxydisulfate Process. *Water* **2022**, *14*, 2811. <https://doi.org/10.3390/w14182811>

Academic Editors: Dionysios (Dion) Demetriou Dionysiou, Yujue Wang and Huijiao Wang

Received: 18 August 2022

Accepted: 6 September 2022

Published: 9 September 2022

Publisher's Note: MDPI stays neutral with regard to jurisdictional claims in published maps and institutional affiliations.



Copyright: © 2022 by the authors. Licensee MDPI, Basel, Switzerland. This article is an open access article distributed under the terms and conditions of the Creative Commons Attribution (CC BY) license (<https://creativecommons.org/licenses/by/4.0/>).

1. Introduction

Acyclovir (ACY) and atenolol (ATL), as the typical and most widely used antiviral and β -blocker agents, are frequently adopted against cardiovascular diseases and two common virus infections (herpes simplex and varicella-zoster) [1,2]. ACY and ATL have been frequently detected in different aquatic environments (from ng L⁻¹ to μ g L⁻¹) owing to their scarce biodegradability and widespread usage during the last decade [2–4]. ACY and ATL could not be effectively eliminated by the conventional treatment processes, including precipitation, biodegradation, and flocculation; hence, wastewater treatment plant effluents are regarded as one of the most important pollution resources. Therefore, in order to effectively respond to Green China and Carbon Neutrality [5,6], it is urgent to explore efficient and eco-friendly technologies for the diminution of ACY and ATL in water treatment.

In this sense, the UV/peroxydisulfate process (UV/PDS) has received considerable attention recently due to the in situ generation of sulfate radicals (SO₄^{•-}, 2.5–3.1 V) and

hydroxyl radicals ($\bullet\text{OH}$, 1.8–2.7 V), relatively high stability, the wider operational pH range, and its high mineralization efficiency of organic pollutants [7–11]. To date, many studies have been conducted to investigate the removal efficiencies of diverse pollutants, the effects of main influential parameters, and the identification of reactive species, etc., in the UV/PDS process [12–15]. Liu et al. (2013) compared the degradation performance of ATL in UV/hydrogen peroxide (UV/ H_2O_2) and UV/PDS processes and observed that UV/PDS was superior to UV/ H_2O_2 for efficient ATL degradation due to the longer half-life time of $\text{SO}_4^{\bullet-}$ and its higher reactivity with ATL than $\bullet\text{OH}$ [3]. Although the removal efficiencies of diverse micropollutants in the UV/PDS process have been widely investigated, limited reports have taken note of the contributions and reaction mechanisms of $\text{SO}_4^{\bullet-}$ and $\bullet\text{OH}$ under different operational conditions.

On the basis of previous studies, the degradation of pollutants in the UV/PDS process is mainly attributed to $\bullet\text{OH}$, $\text{SO}_4^{\bullet-}$, and UV direct photolysis [9,12,16]. In order to accurately investigate the contributions and reaction mechanisms of $\text{SO}_4^{\bullet-}$ and $\bullet\text{OH}$ in the UV/PDS system, the microfluid-based UV reaction system (MVPS) was deployed in this study. The MVPS system, with the advantages of a small total volume, minimum waste liquid generation, and controllable reaction rate via radiation flux, could explore the dynamics process in detail and in-depth [17]. Moreover, both the steady-state assumption and the Kintecus model were applied to compare the radical contribution rates. Furthermore, the elucidation of the degradation pathways of ACY and ATL based on density functional theory (DFT) has rarely been reported in the UV/PDS system.

Therefore, the aims of the present study are (1) to explore the degradation performance of ACY and ATL and the effects of influencing factors in the UV/PDS process; (2) to determine the pH-dependent reaction rate constants of $\bullet\text{OH}$ and $\text{SO}_4^{\bullet-}$ with ACY and ATL; (3) to calculate the contributions of $\bullet\text{OH}$ and $\text{SO}_4^{\bullet-}$ at different operational factors via steady-state assumption and the Kintecus software; (4) to elucidate the degradation pathways of ACY and ATL based on DFT and ultra-performance liquid chromatography-tandem quadrupole time-of-flight mass spectrometry (UPLC-QTOF-MS) analysis in the UV/PDS process. It is worth noting that this research would provide some theoretical support and preliminary exploration, especially for the applicability in wastewater for micropollutants abatement relying on the UV/PDS process.

2. Material and Methods

2.1. Chemicals

Sinopharm Chemical Reagent (Shanghai, China) provided the majority of the commonly used experimental drugs. The PDS, humic acid sodium salt, ACY (>99.0%), ATL (>98%), and 5,5-dimethyl-1-pyrrolidine N-oxide (DMPO, >95%) were obtained from Sigma-Aldrich (St. Louis, MO, USA) and Aladdin (Shanghai, China). Methanol (MeOH) and acetonitrile (ACN) were chromatographically pure and supplied by Fisher Scientific (Geel, Belgium). Ultrapure water (>18.2 M Ω cm), obtained from an A10 Milli-Q system (Millipore, Boston, MA, USA), was used in all of the experiments.

2.2. Experimental Procedures

The batch experiments were conducted in the MVPS equipped with a micro-fluorescent silica detector (MFSD) in the present study (Figure S1). The detailed structure and operational parameters were described in the study by Li et al. [17]. The photon fluence rates at 254 nm ($F_{p,o,UV}$) in the MVPS was determined and calculated to be 1.12×10^{-3} Einstein $\text{m}^{-2} \text{s}^{-1}$ in this study, based on the degradation of uridine (0.01 mM) (Text S1, Figure S2) [18].

Before the batch experiments in MVPS, the lamp was warmed for 30 min until the MFSD signal was stabilized. A mixture solution of moderate PDS reagent, ACY and ATL solution, and phosphate buffer (5 mM) was pumped through the UV tube to receive irradiation in MVPS, and the reaction was started. All of the reactions were performed at 20 °C. The samples were withdrawn from the MVPS system at interval times, immediately quenched with $\text{Na}_2\text{S}_2\text{O}_3$ solution, and stored at 4 °C for subsequent analysis.

2.3. Analytical Methods

The e2695 high-performance liquid chromatography (HPLC) system equipped with a Sunfire C18 column (150 mm × 4.6 mm, 5 μm) and a 2489 Vis-UV detector (Waters, Milford, MA, USA) was used to measure the concentrations of ACY and ATL during the photolysis reaction. MeOH and water (*v:v* = 40:60), as the mobile phase with a flow rate of 0.55 mL min⁻¹, were deployed for ACY detection, while phosphate and ACN (*v:v* = 95:5) at a flow rate of 1.0 mL min⁻¹ was used for ATL analysis. DMPO, a spin-trapping reagent, was employed for the identification of radicals for the electron paramagnetic resonance test (EPR, Bruker A-300 spectrometer, Karlsruhe, Baden Wuerttemberg, Germany). Moreover, the UPLC-QTOF-MS system (Agilent, Wilmington, DE, USA) was applied to determine the intermediates of ACY and ATL in the UV/PDS process. The detection parameters of the UPLC-QTOF-MS system are Supplemented in Text S2 in detail.

2.4. Determination of the Second-Order Reaction Rate Constants

The second-order reaction rate constants of ACY and ATL with •OH ($k_{\bullet OH,ACY}$ and $k_{\bullet OH,ATL}$) and $SO_4^{\bullet -}$ ($k_{SO_4^{\bullet -},ACY}$ and $k_{SO_4^{\bullet -},ATL}$) at different pH values were determined using the competitive kinetics method. The p-chlorobenzoic acid (pCBA) ($k_{\bullet OH,pCBA} = 5 \times 10^9 \text{ M}^{-1} \text{ s}^{-1}$) and benzoic acid (BA) ($k_{SO_4^{\bullet -},BA} = 1.2 \times 10^9 \text{ M}^{-1} \text{ s}^{-1}$) were chosen as the competitive chemicals in the UV/H₂O₂ and UV/PDS processes, respectively [19]. The calculation steps and results are depicted in Text S3 and Figures S3–S7.

2.5. Determination of the Relative Contributions of •OH and $SO_4^{\bullet -}$

The degradation of ACY and ATL in the UV/PDS system could be represented as Equations (1) and (2).

$$-\ln \frac{[ACY]_T}{[ACY]_0} = k_{\bullet OH,ACY} \int [\bullet OH] dt + k_{SO_4^{\bullet -},ACY} \int [SO_4^{\bullet -}] dt + k_{PDS,ACY} \int [PDS] dt + k_{UV,ACY} t \quad (1)$$

$$-\ln \frac{[ATL]_T}{[ATL]_0} = k_{\bullet OH,ATL} \int [\bullet OH] dt + k_{SO_4^{\bullet -},ATL} \int [SO_4^{\bullet -}] dt + k_{PDS,ATL} \int [PDS] dt + k_{UV,ATL} t \quad (2)$$

The PDS oxidation and UV direct photolysis are negligible (Figures S8 and S9). Meanwhile, Equations (1) and (2) can be simplified to Equations (3) and (4) on account of the steady-state assumption of the radicals.

$$\begin{aligned} -\ln \frac{[ACY]_T}{[ACY]_0} &\approx k_{\bullet OH,ACY} \int [\bullet OH] dt + k_{SO_4^{\bullet -},ACY} \int [SO_4^{\bullet -}] dt \\ &= (k_{\bullet OH,ACY} [\bullet OH]_{ss} + k_{SO_4^{\bullet -},ACY} [SO_4^{\bullet -}]_{ss}) t \end{aligned} \quad (3)$$

$$\begin{aligned} -\ln \frac{[ATL]_T}{[ATL]_0} &\approx k_{\bullet OH,ATL} \int [\bullet OH] dt + k_{SO_4^{\bullet -},ATL} \int [SO_4^{\bullet -}] dt \\ &= (k_{\bullet OH,ATL} [\bullet OH]_{ss} + k_{SO_4^{\bullet -},ATL} [SO_4^{\bullet -}]_{ss}) t \end{aligned} \quad (4)$$

where $[\bullet OH]_{ss}$ and $[SO_4^{\bullet -}]_{ss}$ represent the steady-state concentrations of •OH and $SO_4^{\bullet -}$, respectively. In addition, the apparent degradation rate constants of ACY and ATL (k_{obs}) would be further simplified to Equations (5)–(7).

$$k_{obs} = k_{\bullet OH,ACY} [\bullet OH]_{ss} + k_{SO_4^{\bullet -},ACY} [SO_4^{\bullet -}]_{ss} \quad (5)$$

$$k_{obs} = k_{\bullet OH,ATL} [\bullet OH]_{ss} + k_{SO_4^{\bullet -},ATL} [SO_4^{\bullet -}]_{ss} \quad (6)$$

$$k_{obs} = k_{exp,\bullet OH} + k_{exp,SO_4^{\bullet -}} \quad (7)$$

Nitrobenzene (NB), a typical probe compound of $\bullet\text{OH}$ ($k_{\bullet\text{OH},\text{NB}} = 3.0 \times 10^9 \text{ M}^{-1} \text{ s}^{-1}$, $k_{\text{SO}_4^{\bullet-},\text{NB}} < 10^6 \text{ M}^{-1} \text{ s}^{-1}$), was used to determine the $[\bullet\text{OH}]_{\text{ss}}$ [20,21] in the UV/PDS process. The $[\bullet\text{OH}]_{\text{ss}}$ during the reaction could be further expressed as Equation (8):

$$k_{\text{obs},\text{NB}} = k_{\bullet\text{OH},\text{NB}}[\bullet\text{OH}]_{\text{ss}} + k_{\text{UV},\text{NB}} \quad (8)$$

where $k_{\text{obs},\text{NB}}$ and $k_{\text{UV},\text{NB}}$ indicate the pseudo-first-order rate constant and the single UV photolysis rate constant (min^{-1}) of NB (Figure S10). $k_{\bullet\text{OH},\text{NB}}$ represents the reaction rate constants of NB with $\bullet\text{OH}$.

2.6. Kinetic Model

In this study, a reaction kinetic model was performed using Kintecus 6.80 software (James C. Ianni, Albuquerque, NM, USA) [22] to simulate the concentrations of ACY, ATL, and reactive radicals in the UV/PDS process on the basis of 150 elementary reactions (Table S1). All of the rate constants of the above reactions were acquired from our determinations, literature, or estimations of similar reactions. The Kintecus model, with its high predictability and accuracy, has been widely used for simulating chemical reaction kinetics in the UV/chlorine [23], UV/H₂O₂ [24,25], and UV/PDS processes [12,25].

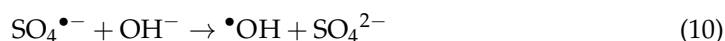
2.7. Quantum Chemistry Calculation

The molecular regioselectivity of ACY and ATL was investigated by the quantum chemical calculation based on DFT. All of the geometry optimizations were implemented at the B3LYP/6–31 G (d) level using the Gaussian 09 program [26]. The wavefunction analysis was carried out at the B3LYP/6–31G (d) level using Multiwfn 3.8 (T. Lu, Beijing, China) [27], based on the structure configuration from the Gaussian optimization. The condensed Fukui function (f^0) was employed as a popular and powerful tool in this study to predict the regioselectivity of ACY and ATL to radical attack at the atomic level. All of the calculation details of f^0 are Supplemented in Text S4.

3. Results and Discussion

3.1. Degradation Efficiencies of ACY and ATL in Different Processes

Figure 1 reveals that the removal of ACY and ATL was significantly promoted in the UV/PDS process with the k_{obs} values of 0.0931 and 0.1938 min^{-1} ($R^2 \geq 0.99$), respectively. However, the ACY and ATL degradation via direct PDS oxidation and UV photolysis can be neglected (Figure 1). The UV/PDS process can produce both $\text{SO}_4^{\bullet-}$ and $\bullet\text{OH}$ due to UV activation of peroxide bond and sulfate conversion [19] (Figure S11) (Equations (9) and (10)) [12,28], resulting in distinct improvement for the elimination of quinolone drugs [29], dyestuff [30], nonsteroidal anti-inflammatory drugs [10], etc.



To verify the roles of $\text{SO}_4^{\bullet-}$ and $\bullet\text{OH}$ for the enhanced ACY and ATL removal, the scavenger experiments were performed in the UV/PDS process (Figure 1). Tertiary butanol (TBA) was used to quench $\bullet\text{OH}$ ($k_{\bullet\text{OH},\text{TBA}} = (3.8\text{--}7.6) \times 10^8 \text{ M}^{-1} \text{ s}^{-1}$ and $k_{\text{SO}_4^{\bullet-},\text{TBA}} = (4.0\text{--}9.1) \times 10^5 \text{ M}^{-1} \text{ s}^{-1}$) [31–33], and MeOH can quench both $\text{SO}_4^{\bullet-}$ and $\bullet\text{OH}$ ($k_{\bullet\text{OH},\text{MeOH}} = 9.7 \times 10^8 \text{ M}^{-1} \text{ s}^{-1}$ and $k_{\text{SO}_4^{\bullet-},\text{MeOH}} = 2.5 \times 10^7 \text{ M}^{-1} \text{ s}^{-1}$) [34–36]. It is notable from Figure 1 that in the presence of TBA and MeOH, the k_{obs} values of ACY degradation reduced by 7.53% and 57.0%, while they declined by 6.73% and 42.0% for ATL, respectively. It is noteworthy from Figure 1 that $\text{SO}_4^{\bullet-}$ instead of $\bullet\text{OH}$ played a vital role in both ATL and ACY degradation in the UV/PDS process. Therefore, it is essential to evaluate the specific contribution rates of $\text{SO}_4^{\bullet-}$ and $\bullet\text{OH}$ for pollutant removal under different parameters in the UV/PDS process.

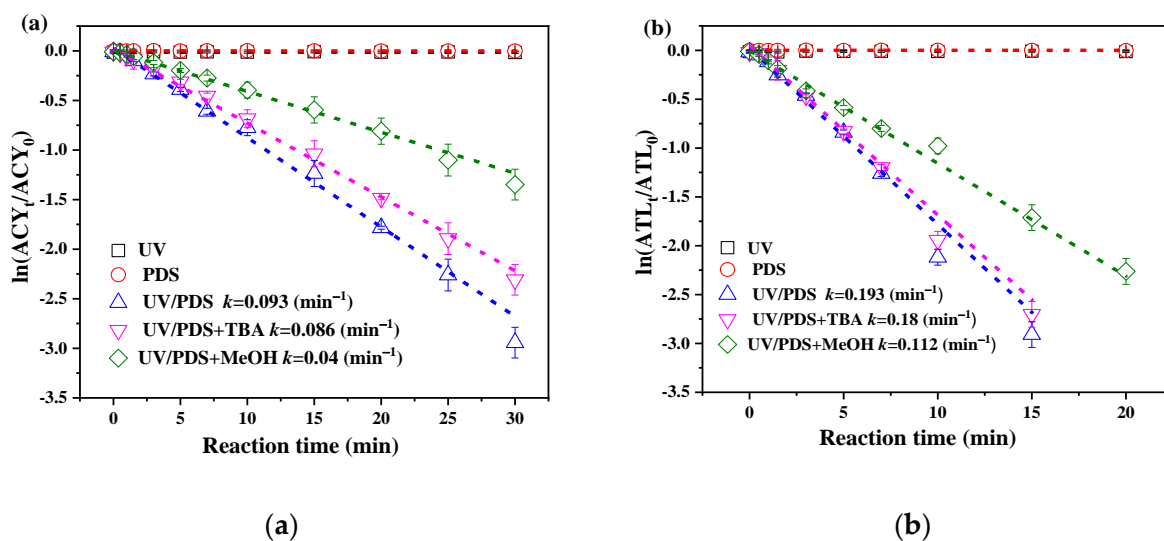


Figure 1. ACY (a) and ATL (b) degradation by UV, PDS, UV/PDS, UV/PDS + TBA, and UV/PDS + MeOH processes. Conditions: $[ACY]_0 = 0.022$ mM, $[ATL]_0 = 0.019$ mM, $[PDS]_0 = 0.6$ mM, $[TBA]_0 = [MeOH]_0 = 10$ mM, pH = 6.0.

3.2. Effects of PDS Dosage

The effects of PDS dosage on the degradation of ACY and ATL were explored and modeled by the Kintecus 6.80 software (James C. Ianni, Albuquerque, NM, USA). As depicted in Figure 2, with the increment in the PDS dosage from 0.1 to 1.0 mM, the degradation of both ACY and ATL was significantly strengthened, and the k_{obs} values of ACY and ATL degradation were promoted from 0.0104 to 0.1213 min^{-1} and 0.0432 to 0.3031 min^{-1} ($R^2 > 0.99$), respectively. The specific rate constants of $\bullet\text{OH}$ and $\text{SO}_4^{\bullet-}$ for ACY and ATL degradation ($k_{exp, \bullet\text{OH}}$ and $k_{exp, \text{SO}_4^{\bullet-}}$) calculated by the steady-state assumption are also presented in Figure 2. The modeled degradation rates of ACY and ATL ($k_{obs, mod}$) highly agreed with the experimental values (k_{obs}) in the UV/PDS process within a credible range (<25%).

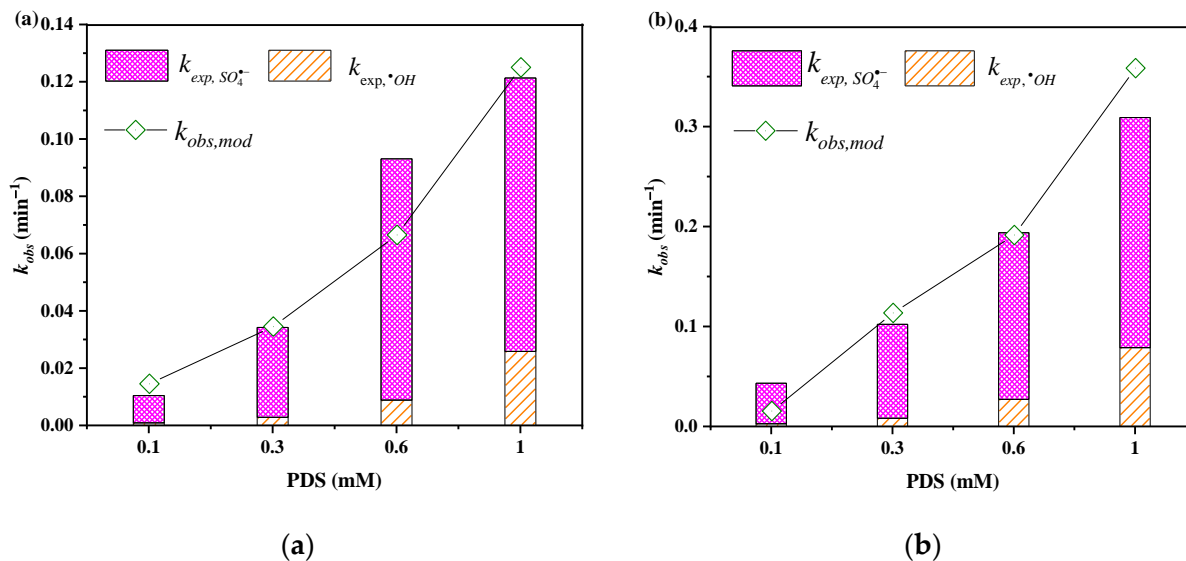


Figure 2. Effects of PDS dosage on the radical contributions and k_{obs} of ACY (a) and ATL (b) in UV/PDS process. Conditions: $[ACY]_0 = 0.022$ mM, $[ATL]_0 = 0.019$ mM, $[PDS]_0 = 0.6$ mM, pH = 6.0.

In addition, it can be noted from Table 1 that the $[\bullet\text{OH}]_{ss}$ and $[\text{SO}_4^{\bullet-}]_{ss}$ in the UV/PDS process gradually increased from 1.00×10^{-14} to 28.72×10^{-14} M and from 1.46

to 8.38×10^{-13} M as the PDS dosage rose from 0.1 to 1.0 mM. Due to the rapid photodecomposition rate of PDS (Figure S12), the yields of both $[\bullet\text{OH}]_{ss}$ and $[\text{SO}_4^{\bullet-}]_{ss}$ in the UV/PDS system were evidently expedited (Table 1) [37], resulting in the gradual increment of the $k_{exp, \bullet\text{OH}}$ and $k_{exp, \text{SO}_4^{\bullet-}}$ values of ACY and ATL (Figure 2). The higher $[\text{SO}_4^{\bullet-}]_{ss}$ led to the higher contribution of $\text{SO}_4^{\bullet-}$ to the degradation of ACY and ATL, manifesting that $\text{SO}_4^{\bullet-}$ rather than $\bullet\text{OH}$ played a major role in pollutant removal. It can be obviously seen from Figure 2 that the modeled results ($k_{obs, mod}$) derived from the kinetic model were in good agreement with the experimental values (k_{obs}) in most cases.

Table 1. $[\bullet\text{OH}]_{ss}$ and $[\text{SO}_4^{\bullet-}]_{ss}$ in UV/PDS process at different PDS dosages and pHs.

Radical Species (M)	PDS (mM)					pH		
	0.1	0.3	0.6	1.0	6.0	9.0	10.0	11.0
$[\bullet\text{OH}]_{ss} \times 10^{-14}$	1.00	3.00	9.83	28.72	9.44	12.27	17.72	17.86
$[\text{SO}_4^{\bullet-}]_{ss} \times 10^{-13}$	1.46	3.39	6.03	8.38	6.13	3.83	2.66	1.79

3.3. Effects of Solution pH

The $k_{\bullet\text{OH}, \text{ACY}}, k_{\text{SO}_4^{\bullet-}, \text{ACY}}, k_{\bullet\text{OH}, \text{ATL}}$, and $k_{\text{SO}_4^{\bullet-}, \text{ATL}}$ values at pH 6.0–11.0 were determined based on the competition kinetics, and the results are depicted in Figure 3. The $k_{\bullet\text{OH}, \text{ACY}}$ and $k_{\text{SO}_4^{\bullet-}, \text{ACY}}$ values declined from 1.50×10^9 to 1.30×10^9 $\text{M}^{-1} \text{s}^{-1}$ and from 1.58×10^9 to 1.00×10^9 $\text{M}^{-1} \text{s}^{-1}$, respectively, with the pH value rising from 6.0 to 11.0 (Figure 3a,b). Russo et al. reported the $k_{\bullet\text{OH}, \text{ACY}}$ to be 2.3×10^9 $\text{M}^{-1} \text{s}^{-1}$ at pH 6.0 [2], and the $k_{\bullet\text{OH}, \text{ACY}}$ and $k_{\text{SO}_4^{\bullet-}, \text{ACY}}$ values at different pHs have been seldom investigated. For ATL (Figure 3c,d), with the increment of pH (6.0–11.0), the $k_{\bullet\text{OH}, \text{ATL}}$ decreased from 4.6×10^9 to 4.11×10^9 $\text{M}^{-1} \text{s}^{-1}$, while the $k_{\text{SO}_4^{\bullet-}, \text{ATL}}$ increased from 4.56×10^9 to 5.64×10^9 $\text{M}^{-1} \text{s}^{-1}$. The pH dependency of the second-order reaction rate constant could be ascribed to a combination of various effects due to the reaction of free radicals ($\bullet\text{OH}$ and $\text{SO}_4^{\bullet-}$) with dissimilar pollutant species, which are the significant parameters of the following kinetic study.

As shown in Figure 4, with the increase in the solution pH from 6.0 to 11.0, the k_{obs} of ACY and ATL distinctly declined from 0.0931 to 0.071 min^{-1} and 0.1938 to 0.101 min^{-1} , respectively, and the $k_{obs, mod}$ were consistent with the experimental results. Additionally, as the pH increased from 6.0 to 11.0, the $k_{exp, \bullet\text{OH}}$ slightly enhanced from 0.00878 to 0.01378 min^{-1} for ACY degradation and from 0.02607 to 0.04357 min^{-1} for ATL degradation, respectively. However, the overt reduction in $k_{exp, \text{SO}_4^{\bullet-}}$ for ACY and ATL degradation was observed. The $k_{exp, \text{SO}_4^{\bullet-}}$ of ACY and ATL decreased by 30.59% and 63.79%, respectively (Figure 4).

Moreover, the $[\bullet\text{OH}]_{ss}$ and $[\text{SO}_4^{\bullet-}]_{ss}$ exhibited similar change patterns with the $k_{exp, \bullet\text{OH}}$ and $k_{exp, \text{SO}_4^{\bullet-}}$ (Table 1). It is notable that the $[\bullet\text{OH}]_{ss}$ obviously increased from 9.44×10^{-14} to 17.86×10^{-14} M, while the $[\text{SO}_4^{\bullet-}]_{ss}$ reduced from 6.13 to 1.79×10^{-13} M with the increasing pH from 6.0 to 11.0 in the UV/PDS processes. Guan et al. (2011) [38] discovered that when the solution pH > 9.3, the distinct fast conversion of $\text{SO}_4^{\bullet-}$ to $\bullet\text{OH}$ caused the declining formation rate of $\text{SO}_4^{\bullet-}$ from photolysis of peroxymonosulfate (PMS) and the reduction in the oxidative power, which were in agreement with the changes of $[\bullet\text{OH}]_{ss}$ and $[\text{SO}_4^{\bullet-}]_{ss}$ in the current study. Liu et al. 2013 [3] investigated the elimination of ATL in the UV/PDS process with a pH range of 3.0–11.0 and discovered the declined degradation rate of ATL with the pH decreasing from 7.0 to 9.0. Furthermore, the reaction of OH^- with $\text{SO}_4^{\bullet-}$ by Equation (10) at high pH, could also result in the decreasing trend of $\text{SO}_4^{\bullet-}$ [29].

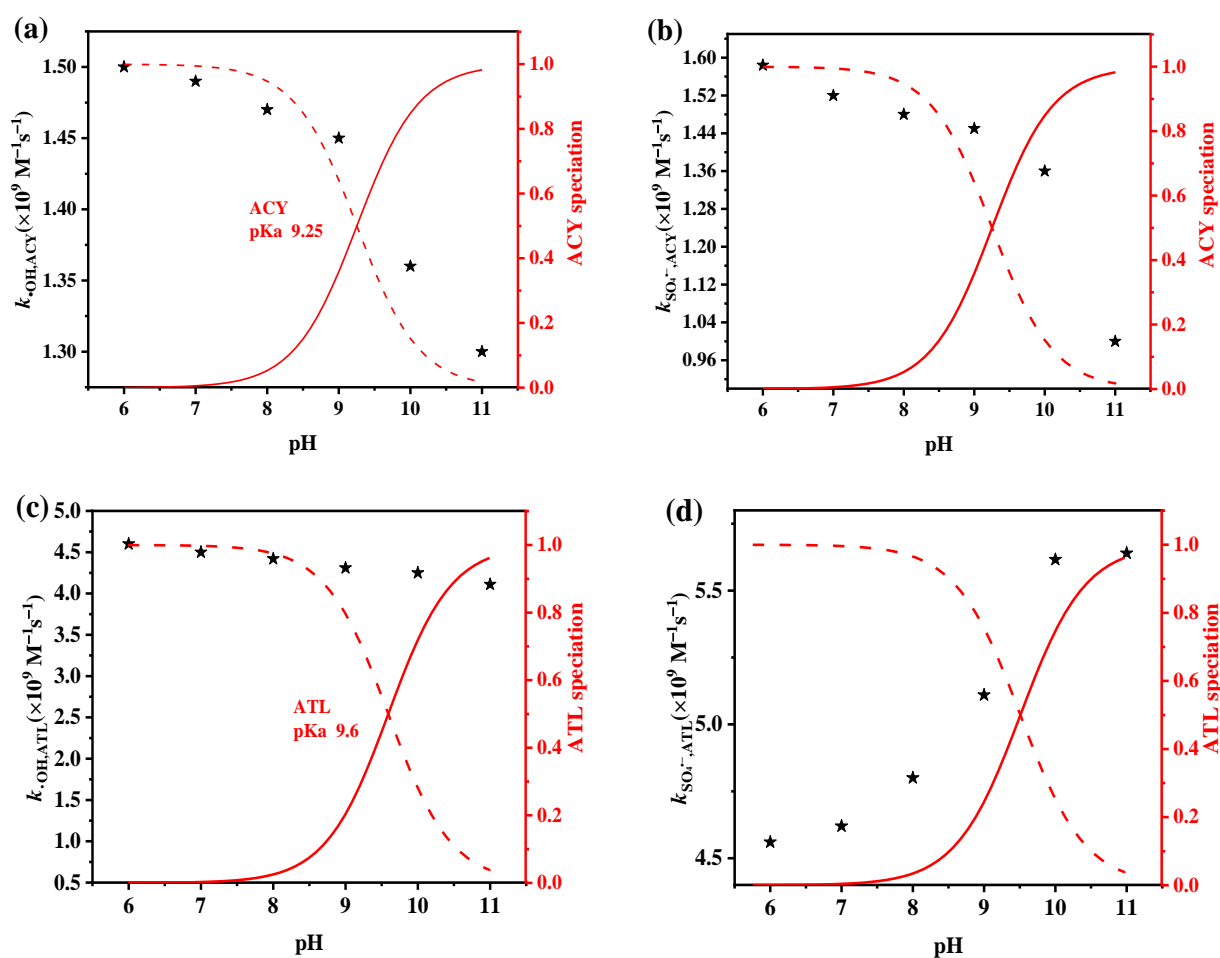


Figure 3. The second-order rate constants of $k_{OH,ACY}$ (a) $k_{SO_4^-,ACY}$ (b), $k_{OH,ATL}$ (c), and $k_{SO_4^-,ATL}$ (d) under different pHs. (black star, measured k ; red lines, speciation). Conditions: $[ACY]_0 = 0.022$ mM, $[ATL]_0 = 0.019$ mM, $[PDS]_0 = 0.6$ mM, pH = 6.0.

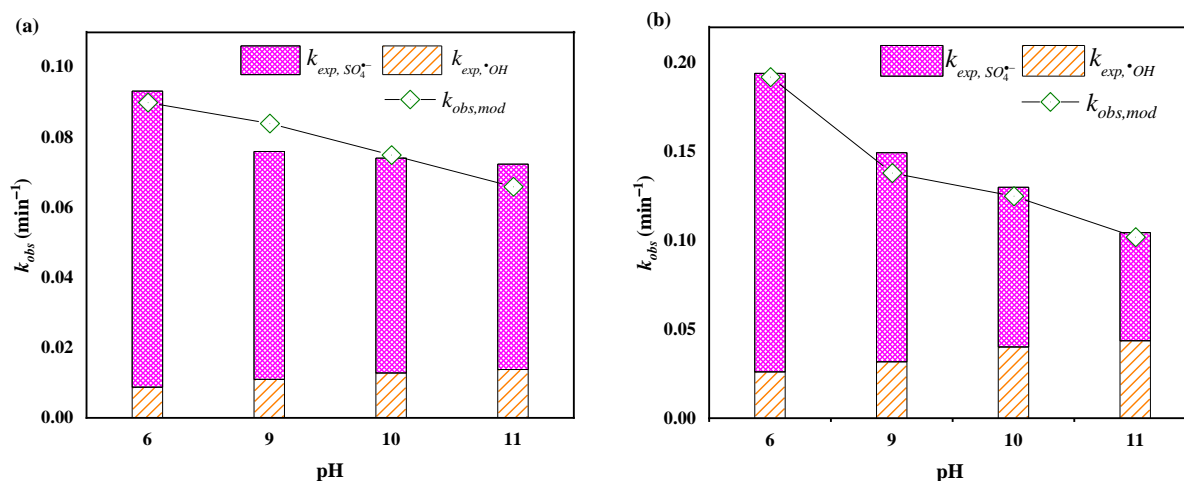


Figure 4. Effects of solution pHs on the radical contributions and k_{obs} of ACY (a) and ATL (b) in UV/PDS process. Conditions: $[ACY]_0 = 0.022$ mM, $[ATL]_0 = 0.019$ mM, $[PDS]_0 = 0.6$ mM.

3.4. Effects of Operation Parameters in UV/PDS Process

3.4.1. Chloride

The existence of Cl^- significantly affected the removal efficiencies of ACY and ATL in the UV/PDS process (Figure 5). As shown in Figure 5a,b, the k_{obs} of ACY and ATL

decreased by 36.56% and 53.36%, with augmenting Cl^- concentration from 0 to 3 mM. Additionally, the $k_{\text{mod},\bullet\text{OH}}$ increased by 62.0–344.4% and $k_{\text{mod},\text{SO}_4^{\bullet-}}$ declined by 82.7–85.1% in the presence of 3 mM Cl^- , respectively. With the augmentation of the Cl^- concentration from 0.5 to 3 mM, the $[\bullet\text{OH}]_{\text{ss}}$ gradually increased from 6.62×10^{-14} to 32.24×10^{-14} M, while the $[\text{SO}_4^{\bullet-}]_{\text{ss}}$ decreased from 4.52×10^{-13} to 1.38×10^{-13} M for ACY and ATL degradation (Table S2). Lutze et al. [23] reported that $\text{SO}_4^{\bullet-}$ would be converted to $\bullet\text{OH}$ in the presence of Cl^- at $\text{pH} \geq 5.0$ (Equations (11)–(15)). Cl^- can react quickly with $\bullet\text{OH}$ to form $\text{ClOH}^{\bullet-}$ with a rate constant of $4.3 \times 10^9 \text{ M}^{-1} \text{ s}^{-1}$ (Equation (13), reverse). In addition, the extremely rapid decomposition rate constant of $\text{ClOH}^{\bullet-}$ ($6.1 \times 10^9 \text{ M}^{-1} \text{ s}^{-1}$, Equation (13)) can obviously suppress the reaction between Cl^- and $\bullet\text{OH}$. However, only at $\text{pH} < 3.0$ did the yield of Cl^\bullet from the reaction of $\text{ClOH}^{\bullet-}$ with H^+ become important (Equation (14)) [39,40]. Noteworthy, the reactions between Cl^- and $\bullet\text{OH}/\text{SO}_4^{\bullet-}$ could also produce several reactive chlorine species ($\text{Cl}^\bullet, \text{Cl}_2^{\bullet-}, \text{ClO}^\bullet$, etc.).

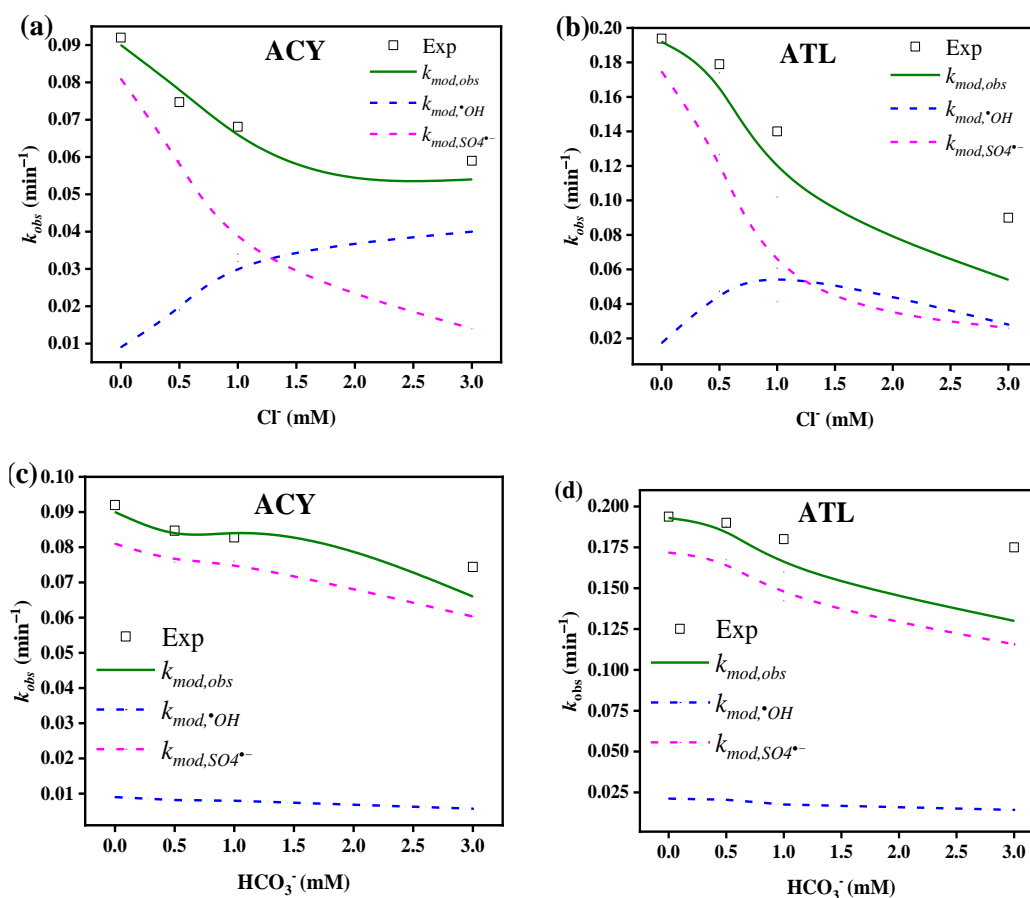
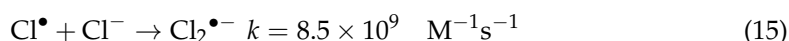
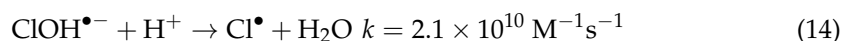
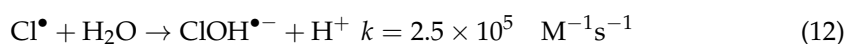


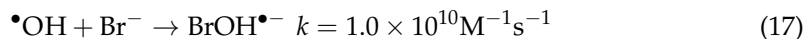
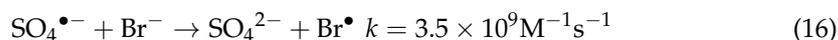
Figure 5. Effects of Cl^- and HCO_3^- dosages on the k_{obs} of ACY (a,c) and ATL (b,d) degradation and specific rates of $\bullet\text{OH}$ and $\text{SO}_4^{\bullet-}$ in UV/PDS process. Conditions: $[\text{ACY}]_0 = 0.022 \text{ mM}$, $[\text{ATL}]_0 = 0.019 \text{ mM}$, $[\text{PDS}]_0 = 0.6 \text{ mM}$, $\text{pH} = 6.0$.

3.4.2. Bicarbonate

It can be seen from Figure 5c,d that the k_{obs} for the abatement of ACY and ATL declined by 8.8–11.82% with the addition of 3 mM HCO_3^- in the UV/PDS system. HCO_3^- can react quickly with $\bullet\text{OH}$ ($8.5 \times 10^6 \text{ M}^{-1} \text{ s}^{-1}$) and $\text{SO}_4^{\bullet-}$ ($1.6 \times 10^6 \text{ M}^{-1} \text{ s}^{-1}$) to form secondary free radical $\text{CO}_3^{\bullet-}$ [6,41], leading to the scavenging effects of $\bullet\text{OH}$ and $\text{SO}_4^{\bullet-}$. Furthermore, the presence of 3 mM HCO_3^- caused $k_{\text{mod},\bullet\text{OH}}$ and $k_{\text{mod},\text{SO}_4^{\bullet-}}$ to decrease by 32.6–36.6% and 25.5–32.6%, respectively. Moreover, at pH 6.0, both H_2CO_3 and HCO_3^- ($pK_{a1} = 6.3$, $pK_{a2} = 10.3$) reacted with $\text{SO}_4^{\bullet-}$ in an analogous rate constant [42–44]. According to the simulation results (Table S2), $[\bullet\text{OH}]_{\text{ss}}$ and $[\text{SO}_4^{\bullet-}]_{\text{ss}}$ distinctly decreased by 6.67%–5.69% and 7.08%–3.77% as the HCO_3^- concentration rose from 0.5 to 3 mM, respectively, resulting in the obvious reduction in the degradation rates of ACY and ATL.

3.4.3. Bromide

It can be observed from Figure 6a,b that the addition of Br^- inhibited the removal efficiencies of ACY and ATL in the UV/PDS process. The k_{obs} for ACY and ATL degradation decreased by 37.7 and 61.14%, respectively, as the Br^- concentration increased from 0 to 1.0 mM. Furthermore, $k_{\text{mod},\bullet\text{OH}}$ and $k_{\text{mod},\text{SO}_4^{\bullet-}}$ decreased by 2.6–66.1% and 51.5–75.1% with the addition of 1.0 mM Br^- . Because Br^- exhibits higher rate constants reacting with $\text{SO}_4^{\bullet-}$ and $\bullet\text{OH}$ (Equations (16) and (17)) than ACY and ATL do, it can be considered a scavenger of $\text{SO}_4^{\bullet-}$ and $\bullet\text{OH}$, which may be the main reason for the decreased removal efficiencies of ACY and ATL. In addition, Lu et al. 2016 [45] also observed that the presence of Br^- notably suppressed the removal of o-phthalic acid (PA) in $\text{SO}_4^{\bullet-}$ -based advanced oxidation systems, and PA probably did not react with the generated reactive bromide species directly.



3.4.4. NOM

It can be observed from Figure 6c,d that the natural organic matter (NOM) markedly inhibited the removal efficiencies of ACY and ATL in the UV/PDS process. It is worth noting that the k_{obs} for ACY and ATL significantly dropped by 36.6% and 50.9% with the addition of 3.0 mgC L^{-1} NOM. Meanwhile, the $k_{\text{mod},\bullet\text{OH}}$ and $k_{\text{mod},\text{SO}_4^{\bullet-}}$ decreased by 35.3–57.8% and 25.7–56.3%, respectively, under the same conditions (3 mgC L^{-1} NOM). It is noted from Figure 6 that the experimental k_{obs} for the abatement of ACY and ATL were highly compliant with the simulated results. It is well known that NOM can react with $\bullet\text{OH}$ ($1.4 \times 10^4 \text{ L mgC}^{-1} \text{ s}^{-1}$) and $\text{SO}_4^{\bullet-}$ ($6.8 \times 10^3 \text{ L mgC}^{-1} \text{ s}^{-1}$), resulting in their reduction [23]. Furthermore, NOM could act as an inner filter of UV light affecting the yields of $\bullet\text{OH}$ and $\text{SO}_4^{\bullet-}$ derived from direct photolysis of PDS [44,46].

3.4.5. Sulfate and Nitrate

It can be seen in Figure S13 that the abatement of ACY and ATL in the UV/PDS process was markedly restrained by the addition of SO_4^{2-} . The k_{obs} for ACY and ATL decreased by 15.1% and 13.8%, respectively, when the concentration of SO_4^{2-} increased to 3 mM. In addition, the $k_{\text{mod},\bullet\text{OH}}$ and $k_{\text{mod},\text{SO}_4^{\bullet-}}$ decreased by 18.6–35.3% and 19.2–33.1% in the presence of 3 mM SO_4^{2-} . Furthermore, we can intuitively find that the experimental values are consistent with the simulated values. The higher concentration of SO_4^{2-} could induce the reductions of the redox potential of $\text{SO}_4^{\bullet-}/\text{SO}_4^{2-}$ and the oxidation capacity of the UV/PDS process on the basis of the Nernst equation (Equations (18) and (19)) [47,48]. Whereas $\text{SO}_4^{\bullet-}$ could also be formed through the reaction of $\bullet\text{OH}$ with SO_4^{2-} (Equation (20)). How-

ever, the lower reaction rate constants of $\text{SO}_4^{\bullet-}$ with ACY/ATL than $\bullet\text{OH}$ would lead to suppressive effects on the k_{obs} of ACY and ATL degradation.



$$E_{(\text{SO}_4^{\bullet-}/\text{SO}_4^{2-})} = E^{\theta}_{(\text{SO}_4^{\bullet-}/\text{SO}_4^{2-})} + \frac{RT}{zF} \ln \frac{[\text{SO}_4^{\bullet-}]}{[\text{SO}_4^{2-}]} \tag{19}$$

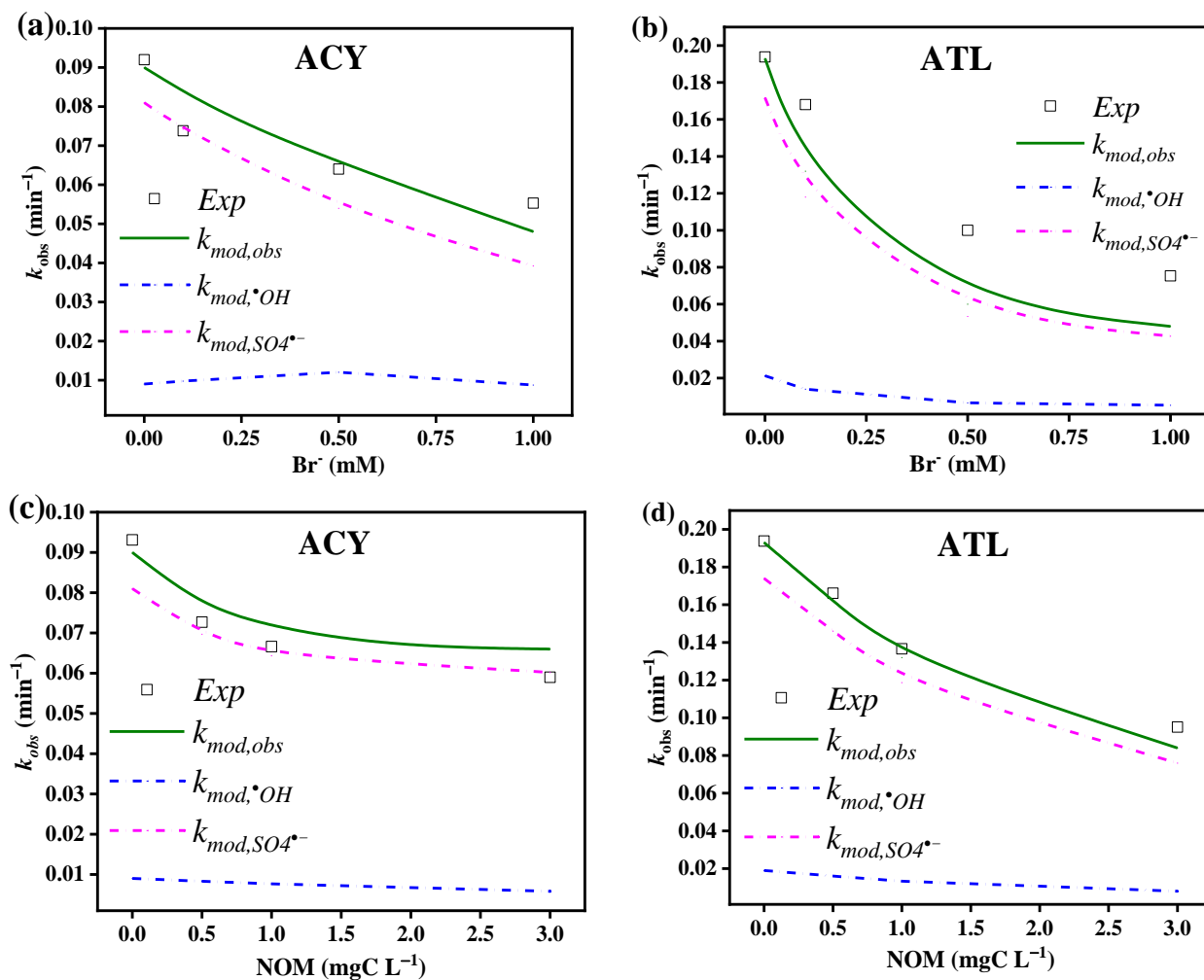


Figure 6. Effect of Br^- dosage and NOM on the k_{obs} of ACY (a,c) and ATL (b,d) degradation and specific rates of $\bullet\text{OH}$ and $\text{SO}_4^{\bullet-}$ in UV/PDS process. Conditions: $[\text{ACY}]_0 = 0.022 \text{ mM}$, $[\text{ATL}]_0 = 0.019 \text{ mM}$, $[\text{PDS}]_0 = 0.6 \text{ mM}$, $\text{pH} = 6.0$.

NO_3^- (0.5–3 mM) visibly inhibited the removal efficiencies of ACY and ATL in the UV/PDS system (Figure S14). The k_{obs} for ACY and ATL decreased by 26.0% and 27.7%, as the NO_3^- concentration rose to 3 mM. The $k_{\text{mod},\bullet\text{OH}}$ and $k_{\text{mod},\text{SO}_4^{\bullet-}}$ decreased by 18.6–37.1% and 19.2–36.3% in the presence of 3 mM NO_3^- , respectively. NO_3^- can be used as a photosensitizer, consuming UV_{254} during the reaction. Wang et al. demonstrated the strong inhibition of NO_3^- on the degradation of TAP in the UV/PDS system [49]. Lin et al. revealed that NO_3^- can significantly reduce the radiation intensity received by PMS, thereby slowing down the degradation of BPA [21].

3.5. Oxidation Mechanisms and Degradation Pathways Speculation

The f^0 of ACY and ATL based on the Hirshfeld charge was calculated using Multiwfn software [46,50,51], and the results are represented in Tables S3 and S4 and Figures 7 and 8. Moreover, Tables S5 and S6 tabulated the reasonable transformation products (TPs) of ACY and ATL [52,53], which were detected by UPLC-QTOF-MS.

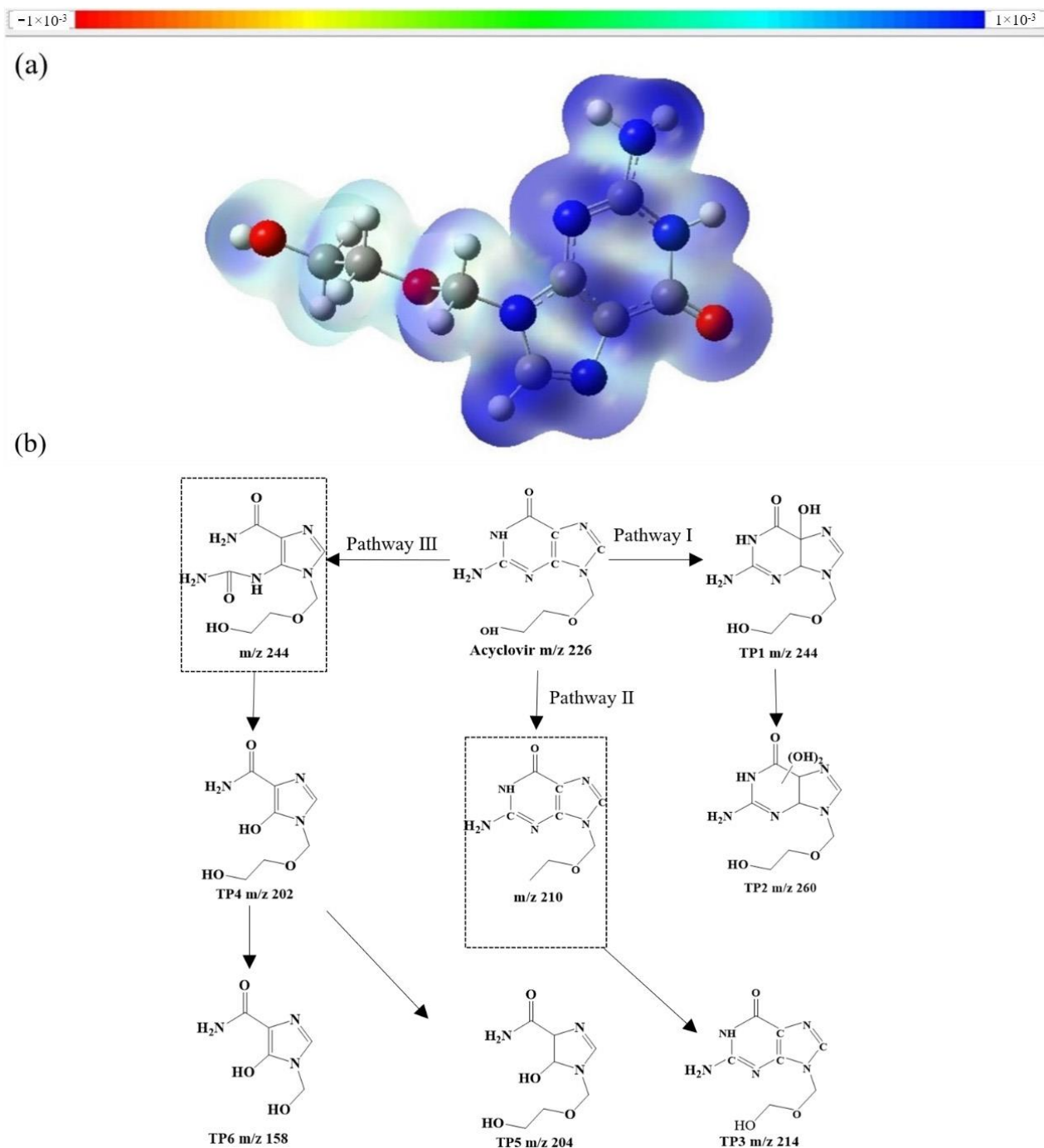


Figure 7. The contour surfaces of Fukui function f^0 for ACY with isovalue of 0.01 (a) and the plausible transformation pathways of ACY in UV/PDS process (b). Conditions: $[ACY]_0 = 0.022$ mM, $[PDS]_0 = 0.6$ mM, pH = 6.0.

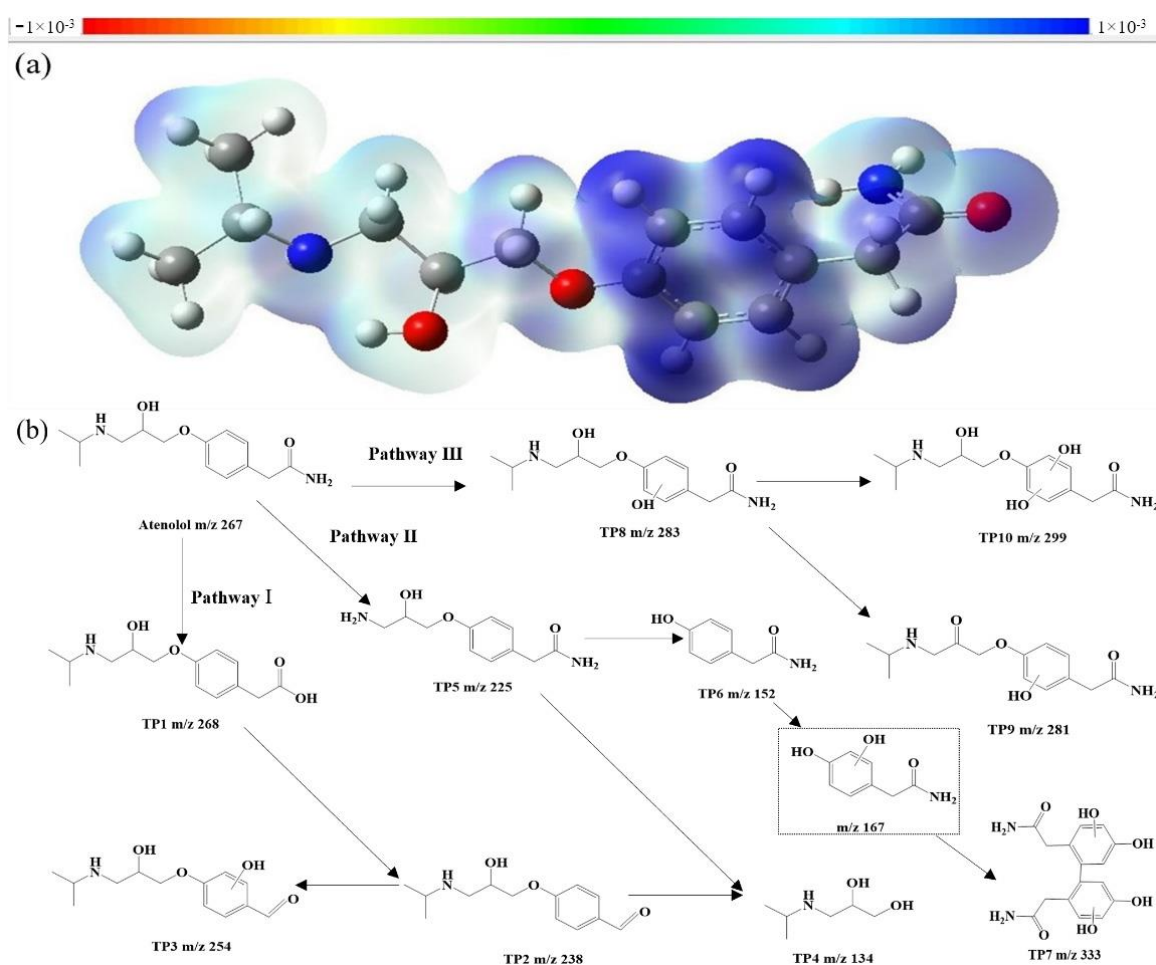


Figure 8. The contour surfaces of Fukui function f^0 for ATL with isovalue of 0.01 (a) and the plausible transformation pathways of ATL in UV/PDS process (b). Conditions: $[\text{ATL}]_0 = 0.022 \text{ mM}$, $[\text{PDS}]_0 = 0.6 \text{ mM}$, $\text{pH} = 6.0$.

According to the results in Table S3 and Figure 7a, the highest values of f^0 (blue area in Figure 7a) were achieved in the C1, C2, C5, C8, N6, N16, and O15 positions of ACY (Figure S15a), which were much easier to be attacked by $\bullet\text{OH}$ and/or $\text{SO}_4^{\bullet-}$. An et al. [54] also found similar degradation patterns for ACY, and the dominating reaction pathway of ACY with $\bullet\text{OH}$ initiated by the addition onto the ortho site of methoxy substituent on the benzene ring (i.e., C1 and C2 positions in this study). As shown in Figure 7b, combining the six detected transformation intermediates (Table S5) and the results of the Fukui function calculations, three degradation pathways for ACY in the UV/PDS process were proposed. Pathway I underwent the electrophilic addition reaction through $\bullet\text{OH}$ attacking the ACY N-heterocycle, resulting in the formation of the hydroxylated products TP1 and TP2 through dihydroxylation. Pathway II: ACY may also transform to TP3 through a de-alcoholic reaction and subsequent hydroxylation. Pathway III: The C5 and N6 could be further attacked by $\bullet\text{OH}$ and $\text{SO}_4^{\bullet-}$, further causing ring opening and the production of TP4 through further hydroxylation. Then, TP4 could generate TP5 through H addition or TP6 by de-alcoholic reaction and hydroxylation.

It can be observed from Table S4 and Figure 8a that the $\bullet\text{OH}/\text{SO}_4^{\bullet-}$ radicals most favorably attack the C5, C6, C7, C18, C19, O1, and O9 positions of ATL (Figure S15b). In addition, Miao et al. [55] also reported that $\bullet\text{OH}$ would most likely attack the C3 position of ATL (i.e., the C6 position in this study) to produce hydroxylation products. In addition, Miao et al. [55] also reported that the atom with a higher $2\text{FED}_{\text{HOMO}}^2$ value in the ATL structure was the O11 position (i.e., O9 position in this study), indicating that the breaking

of the ether bond is reasonable. Herein, three plausible transformation pathways of ATL (Figure 8b) on the basis of the 10 transformation products (Table S6) were as follows. Pathway I: the oxidation of the primary amide group in the main side chain would lead to the formation of TP1 with m/z 268. Subsequently, the addition of oxygen to the alkyl group and hydrogen abstraction by $\bullet\text{OH}$ contributed to the generation of TP2 and was further hydroxylated to produce TP3. $\bullet\text{OH}/\text{SO}_4^{\bullet-}$ can attack ether linkage and undergo cleavage of ether linkage to form TP4 with m/z 134. Pathway II: The secondary amine structure of ATL could be attacked by $\bullet\text{OH}/\text{SO}_4^{\bullet-}$, causing the cleavage of the C–N bond to produce TP5. Afterward, TP4 and TP6 could also be attributed to the split of the ether linkage caused by the attack of $\bullet\text{OH}/\text{SO}_4^{\bullet-}$. After that, the reaction initiated at the secondary amine moieties (–NH–) and dimerization would lead to the yield of TP7. Pathway III revealed the electrophilic addition reaction through $\bullet\text{OH}$ attacking the ATL aromatic ring, producing the hydroxylated product TP8, which was then carbonylated to generate TP9 and hydroxylated to TP10.

4. Conclusions

In summary, the degradation of ACY and ATL derived from $\text{SO}_4^{\bullet-}$ and $\bullet\text{OH}$ in the UV/PDS process was comprehensively investigated concerning kinetic simulations and degradation mechanisms. The second-order rate constants at 6.0–11.0 for ACY and ATL reacting with $\bullet\text{OH}$ were estimated to be 1.30–1.50 and 3.45–4.60 $\text{M}^{-1}\text{s}^{-1}$, and those for ACY and ATL with $\text{SO}_4^{\bullet-}$ were 1.00–1.58 and 4.56–5.64 $\text{M}^{-1}\text{s}^{-1}$, respectively. In addition, the radical quenching experiments and the steady-state assumption calculation demonstrated that $\text{SO}_4^{\bullet-}$ instead of $\bullet\text{OH}$ was the predominant radical for pollutant elimination in the UV/PDS process. Additionally, the kinetic model deployed in the current study could well predict the degradation rates of ACY and ATL under different operational parameters. The degradation rates of $\bullet\text{OH}$ and $\text{SO}_4^{\bullet-}$ for ACY and ATL degradation were highly pH-dependent. Based on the prediction of the active sites via the Fukui function and the intermediates of ACY and ATL identified by UPLC-QTOF-MS, the plausible transformation pathways of ACY and ATL in the UV/PDS process have been proposed. This study could provide some theoretical support and preliminary exploration for pollutant removal in the UV/PDS system. Furthermore, the toxicity of the target pollutants and their intermediates in the UV/PDS system could be considered in future studies.

Supplementary Materials: The following supporting information can be downloaded at: <https://www.mdpi.com/article/10.3390/w14182811/s1>, Text S1. Determination of $F_{p,o,UV}$ in the MVPS; Text S2. UPLC-QTOF-MS method; Text S3. Determination of the second-order reaction rate constants; Text S4. Calculation of condensed Fukui function; Table S1: Principal reactions and rate constants in the UV/PDS system; Table S2: Modeled steady-state concentrations of $\bullet\text{OH}$ and $\text{SO}_4^{\bullet-}$ in different water matrices; Table S3: Calculated condensed Fukui function and dual descriptor of ACY; Table S4: Calculated condensed Fukui function and dual descriptor of ATL; Table S5: Major intermediates of ACY detected in UV/PDS process; Table S6: Major intermediates of ATL detected in UV/PDS process; Figure S1: Schematic diagram of the MVPS; Figure S2: The degradation of uridine under direct UV photolysis; Figure S3: Determination of the second-order rate constant for the reaction of ACY with $\bullet\text{OH}$ at pH = 6.0 (a), pH = 9.0 (b), and pH = 11.0 (c); Figure S4: Determination of the second-order rate constant for the reaction of ACY with $\text{SO}_4^{\bullet-}$ at pH = 6.0 (a), pH = 9.0 (b), and pH = 11.0 (c); Figure S5: Determination of the second-order rate constant for the reaction of ATL with $\bullet\text{OH}$ at pH = 6.0 (a), pH = 9.0 (b), and pH = 11.0 (c); Figure S6: Determination of the second-order rate constant for the reaction of ATL with $\text{SO}_4^{\bullet-}$ at pH = 6.0 (a), pH = 9.0 (b), and pH = 11.0 (c); Figure S7: The existence forms of competing substrates pCBA(a) and BA(b) at different pH; Figure S8: Determination of ACY by UV irradiation (a) and PDS oxidation (b) at different pH; Figure S9: Determination of ATL by UV irradiation (a) and PDS oxidation (b) at different pH; Figure S10: The apparent degradation rate constants of NB in direct UV photolysis and UV/PDS processes at different pHs; Figure S11: EPR spectra of $\bullet\text{OH}$ and $\text{SO}_4^{\bullet-}$ adducts in UV/PDS process; Figure S12: Attenuation of PDS in UV/PDS process for the degradation of ACY (a) and ATL (b); Figure S13: Effect of SO_4^{2-} dosage on the kobs of ACY (a) and ATL (b) degradation and specific

rates of $\bullet\text{OH}$ and $\text{SO}_4^{\bullet-}$ in the UV/PDS process; Figure S14: Effect of NO_3^- dosage on the k_{obs} of ACY (a) and ATL (b) degradation and specific rates of $\bullet\text{OH}$ and $\text{SO}_4^{\bullet-}$ in UV/PDS process; Figure S15: Structural formula of ACY(a) and ATL (b) [56–74].

Author Contributions: Conceptualization, X.Y. and D.X.; methodology, Z.L.; software, H.D.; validation, H.D. and X.Y.; formal analysis, L.S.; investigation, Z.L. and W.Q.; writing—original draft preparation, Z.L.; writing—review and editing, X.Y. and F.P.; supervision, X.Y. and D.X.; funding acquisition, X.Y. All authors have read and agreed to the published version of the manuscript.

Funding: This work was financially supported by the National Natural Science Foundation of China (51808412).

Data Availability Statement: FigShare [<https://doi.org/10.6084/m9.figshare.21067627> (accessed on 17 August 2022)]; FigShare [<https://doi.org/10.6084/m9.figshare.21067618> (accessed on 17 August 2022)].

Acknowledgments: We are very grateful to Jun Men from the analysis and testing center of the Institute of Hydrobiology, Chinese Academy of Sciences with the great help for the identification and analysis of intermediates in this study.

Conflicts of Interest: The authors declare no conflict of interest.

References

1. Yu, X.P.; Qin, W.L.; Yuan, X.J.; Sun, L.; Pan, F.; Xia, D.S. Synergistic mechanism and degradation kinetics for atenolol elimination via integrated UV/ozone/peroxymonosulfate process. *J. Hazard. Mater.* **2021**, *407*, 124393. [[CrossRef](#)] [[PubMed](#)]
2. Russo, D.; Siciliano, A.; Guida, M.; Galdiero, E.; Amoresano, A.; Andreozzi, R.; Reis, N.M.; Puma, G.L.; Marotta, R. Photodegradation and ecotoxicology of acyclovir in water under UV254 and UV254/H₂O₂ processes. *Water Res.* **2017**, *122*, 591–602. [[CrossRef](#)] [[PubMed](#)]
3. Liu, X.; Fang, L.; Zhou, Y.C.; Zhang, T.Q.; Shao, Y. Comparison of UV/PDS and UV/H₂O₂ processes for the degradation of atenolol in water. *J. Environ. Sci.* **2013**, *25*, 1519–1528. [[CrossRef](#)]
4. Liang, C.J.; Wang, Z.S.; Mohanty, N. Influences of carbonate and chloride ions on persulfate oxidation of trichloroethylene at 20 °C. *Sci. Total. Environ.* **2006**, *370*, 271–277. [[CrossRef](#)] [[PubMed](#)]
5. Kranina, E.I. China on the way to achieving carbon neutrality. *Financ. J.* **2021**, *13*, 51–61. [[CrossRef](#)]
6. Bushukina, V.I. Specific features of renewable energy development in the world and russia. *Financ. J.* **2021**, *13*, 93–107. [[CrossRef](#)]
7. Ma, X.; Chen, H.; Chen, R.; Hu, X. Direct and activated chlorine dioxide oxidation for micropollutant abatement: A review on kinetics, reactive sites, and degradation pathway. *Water* **2022**, *14*, 2028. [[CrossRef](#)]
8. Parolini, M.; Pedriali, A.; Binelli, A. Application of a biomarker response index for ranking the toxicity of five pharmaceutical and personal care products (PPCPs) to the bivalve *Dreissena polymorpha*. *Arch. Environ. Contam. Toxicol.* **2013**, *64*, 439–447. [[CrossRef](#)]
9. Lai, F.; Tian, F.X.; Xu, B.; Ye, W.K.; Gao, Y.Q.; Chen, C.; Xing, H.B.; Wang, B.; Xie, M.J.; Hu, X.J. A comparative study on the degradation of phenylurea herbicides by UV/persulfate process: Kinetics, mechanisms, energy demand and toxicity evaluation associated with DBPs. *Chem. Eng. J.* **2022**, *428*, 132088. [[CrossRef](#)]
10. Fu, Y.Y.; Gao, X.S.; Geng, J.J.; Li, S.L.; Wu, G.; Ren, H.Q. Degradation of three nonsteroidal anti-inflammatory drugs by UV/persulfate: Degradation mechanisms, efficiency in effluents disposal. *Chem. Eng. J.* **2019**, *356*, 1032–1041. [[CrossRef](#)]
11. Hou, S.D.; Ling, L.; Shang, C.; Guan, Y.H.; Fang, J.Y. Degradation kinetics and pathways of haloacetonitriles by the UV/persulfate process. *Chem. Eng. J.* **2017**, *320*, 478–484. [[CrossRef](#)]
12. Fu, Y.Y.; Wu, G.; Geng, J.J.; Li, J.C.; Li, S.N.; Ren, H.Q. Kinetics and modeling of artificial sweeteners degradation in wastewater by the UV/persulfate process. *Water Res.* **2019**, *150*, 12–20. [[CrossRef](#)] [[PubMed](#)]
13. Wang, Z.Y.; An, N.; Shao, Y.S.; Gao, N.Y.; Du, E.; Xu, B. Experimental and simulation investigations of UV/persulfate treatment in presence of bromide: Effects on degradation kinetics, formation of brominated disinfection byproducts and bromate. *Sep. Purif. Technol.* **2020**, *242*, 116767. [[CrossRef](#)]
14. Acero, J.L.; Benítez, F.J.; Real, F.J.; Rodríguez, E. Degradation of selected emerging contaminants by UV-activated persulfate: Kinetics and influence of matrix constituents. *Sep. Purif. Technol.* **2018**, *201*, 41–50. [[CrossRef](#)]
15. Li, Q.; Wang, L.F.; Fang, X.H.; Zhang, L.; Li, J.J.; Xie, H.Y. Synergistic effect of photocatalytic degradation of hexabromocyclododecane in water by UV/TiO₂/persulfate. *Catalysts* **2019**, *9*, 189. [[CrossRef](#)]
16. Zhang, Y.Q.; Xiao, Y.J.; Zhong, Y.; Lim, T.T. Comparison of amoxicillin photodegradation in the UV/H₂O₂ and UV/persulfate systems: Reaction kinetics, degradation pathways, and antibacterial activity. *Chem. Eng. J.* **2019**, *372*, 420–428. [[CrossRef](#)]
17. Li, M.K.; Wang, C.; Yau, M.L.; Bolton, J.R.; Qiang, Z.M. Sulfamethazine degradation in water by the VUV/UV process: Kinetics, mechanism and antibacterial activity determination based on a mini-fluidic VUV/UV photoreaction system. *Water Res.* **2017**, *108*, 348–355. [[CrossRef](#)]

18. Li, M.; Li, W.T.; Bolton, J.R.; Blatchley, E.R.; Qiang, Z.M. Organic pollutant degradation in water by the vacuum-ultraviolet/ultraviolet/H₂O₂ process: Inhibition and enhancement roles of H₂O₂. *Environ. Sci. Technol.* **2019**, *53*, 912–918. [[CrossRef](#)]
19. Neghi, N.; Krishnan, N.R.; Kumar, M. Analysis of metronidazole removal and micro-toxicity in photolytic systems: Effects of persulfate dosage, anions and reactor operation-mode. *J. Environ. Chem. Eng.* **2018**, *6*, 754–761. [[CrossRef](#)]
20. Lin, Z.; Qin, W.L.; Sun, L.; Yuan, X.J.; Xia, D.S. Kinetics and mechanism of sulfate radical- and hydroxyl radical-induced degradation of Bisphenol A in VUV/UV/peroxymonosulfate system. *J. Environ. Chem. Eng.* **2020**, *38*, 101636. [[CrossRef](#)]
21. Xiao, Y.J.; Zhang, L.F.; Zhang, W.; Lim, K.Y.; Webster, R.D.; Lim, T.T. Comparative evaluation of iodoacids removal by UV/persulfate and UV/H₂O₂ processes. *Water Res.* **2016**, *102*, 629–639. [[CrossRef](#)] [[PubMed](#)]
22. Lutze, H.V.; Bircher, S.; Rapp, I.; Kerlin, N.; Bakkour, R.; Geisler, M.; von Sonntag, C.; Schmidt, T.C. Degradation of chlorotriazine pesticides by sulfate radicals and the influence of organic matter. *Environ. Sci. Technol.* **2015**, *49*, 1673–1680. [[CrossRef](#)] [[PubMed](#)]
23. Zhao, X.; Jiang, J.; Pang, S.Y.; Guan, C.T.; Li, J.; Wang, Z.; Ma, J.; Luo, C.W. Degradation of iopamidol by three UV-based oxidation processes: Kinetics, pathways, and formation of iodinated disinfection byproducts. *Chemosphere* **2019**, *221*, 270–277. [[CrossRef](#)] [[PubMed](#)]
24. Cong, J.; Wen, G.; Huang, T.L.; Deng, L.Y.; Ma, J. Study on enhanced ozonation degradation of para-chlorobenzoic acid by peroxymonosulfate in aqueous solution. *Chem. Eng. J.* **2015**, *264*, 399–403. [[CrossRef](#)]
25. Li, M.X.; Sun, J.F.; Han, D.D.; Wei, B.; Mei, Q.; An, Z.X.; Wang, X.Y.; Cao, H.J.; Xie, J.; He, M.X. Theoretical investigation on the contribution of •OH, SO₄•⁻ and CO₃•⁻ radicals to the degradation of phenacetin in water: Mechanisms, kinetics, and toxicity evaluation. *Ecotoxicol. Environ. Saf.* **2020**, *204*, 110977. [[CrossRef](#)]
26. Lee, M.; Zimmermann-Steffens, S.G.; Arey, J.S.; Fenner, K.; Gunten, U.V. Development of prediction models for the reactivity of organic compounds with ozone in aqueous solution by quantum chemical calculations: The role of delocalized and localized molecular orbitals. *Environ. Sci. Technol.* **2015**, *49*, 9925–9935. [[CrossRef](#)] [[PubMed](#)]
27. Lu, T.; Chen, F.W. Multiwfn: A multifunctional wavefunction analyzer. *J. Comput. Chem.* **2012**, *33*, 580–592. [[CrossRef](#)]
28. Lee, M.Y.; Wang, W.L.; Xu, Z.B.; Ye, B.; Wu, Q.Y.; Hu, H.Y. The application of UV/PS oxidation for removal of a quaternary ammonium compound of dodecyl trimethyl ammonium chloride (DTAC): The kinetics and mechanism. *Sci. Total. Environ.* **2019**, *655*, 1261–1269. [[CrossRef](#)]
29. Liu, X.H.; Liu, Y.; Lu, S.Y.; Wang, Z.; Wang, Y.Q.; Zhang, G.D.; Guo, X.C.; Guo, W.; Zhang, T.T.; Xi, B.D. Degradation difference of ofloxacin and levofloxacin by UV/H₂O₂ and UV/PS (persulfate): Efficiency, factors and mechanism. *Chem. Eng. J.* **2020**, *385*, 123987. [[CrossRef](#)]
30. Ding, X.X.; Gutierrez, L.; Croue, J.P.; Li, M.; Wang, L.J.; Wang, Y.R. Hydroxyl and sulfate radical-based oxidation of RhB dye in UV/H₂O₂ and UV/persulfate systems: Kinetics, mechanisms, and comparison. *Chemosphere* **2020**, *253*, 126655. [[CrossRef](#)]
31. Yasmeen, H.; Zada, A.; Liu, S.X. Surface plasmon resonance electron channeled through amorphous aluminum oxide bridged ZnO coupled g-C₃N₄ significantly promotes charge separation for pollutants degradation under visible light. *J. Photochem. Photobiol. A Chem.* **2020**, *400*, 112681.
32. Yasmeen, H.; Zada, A.; Liu, S.X. Dye loaded MnO₂ and chlorine intercalated g-C₃N₄ coupling impart enhanced visible light photoactivities for pollutants degradation. *J. Photochem. Photobiol. A Chem.* **2019**, *380*, 111867. [[CrossRef](#)]
33. Zhang, Z.H.; Zada, A.; Cui, N.; Liu, N.W.; Liu, M.H.; Yang, Y.Z.; Jiang, D.L.; Jiang, J.H.; Liu, S.Y. Synthesis of Ag loaded ZnO/BiOCl with high photocatalytic performance for the removal of antibiotic pollutants. *Crystals* **2021**, *11*, 981. [[CrossRef](#)]
34. Anipsitakis, G.P.; Dionysiou, D.D. Transition metal/UV-based advanced oxidation technologies for water decontamination. *Appl. Catal. B Environ.* **2004**, *54*, 155–163. [[CrossRef](#)]
35. Lescano, M.R.; Lopez, A.O.; Romero, R.L.; Zalazar, C.S. Degradation of chlorpyrifos formulation in water by the UV/H₂O₂ process: Lumped kinetic modelling of total organic carbon removal. *J. Photochem. Photobiol. A* **2021**, *404*, 112924. [[CrossRef](#)]
36. Yoon, S.H.; Jeong, S.; Lee, S. Oxidation of bisphenol A by UV/S₂O₈²⁻: Comparison with UV/H₂O₂. *Environ. Technol.* **2012**, *33*, 123–128. [[CrossRef](#)]
37. He, X.X.; Mezyk, S.P.; Michael, I.; Fatta-Kassinos, D.; Dionysiou, D.D. Degradation kinetics and mechanism of beta-lactam antibiotics by the activation of H₂O₂ and Na₂S₂O₈ under UV-254nm irradiation. *J. Hazard. Mater.* **2014**, *279*, 375–383. [[CrossRef](#)]
38. Guan, Y.H.; Ma, J.; Li, X.C.; Fang, J.Y.; Chen, L.W. Influence of pH on the formation of sulfate and hydroxyl radicals in the UV/peroxymonosulfate system. *Environ. Sci. Technol.* **2011**, *45*, 9308–9314. [[CrossRef](#)]
39. Yang, Y.; Pignatello, J.J.; Ma, J.; Mitch, W.A. Comparison of halide impacts on the efficiency of contaminant degradation by sulfate and hydroxyl radical-based advanced oxidation processes (AOPs). *Environ. Sci. Technol.* **2014**, *48*, 2344–2351. [[CrossRef](#)]
40. Gunten, U.V. Ozonation of drinking water: Part II. Disinfection and by-product formation in presence of bromide, iodide or chlorine. *Water Res.* **2003**, *37*, 1469–1487. [[CrossRef](#)]
41. Lu, X.; Shao, Y.S.; Gao, N.Y.; Chen, J.X.; Zhang, Y.S.; Xiang, H.M.; Guo, Y.L. Degradation of diclofenac by UV-activated persulfate process: Kinetic studies, degradation pathways and toxicity assessments. *Ecotoxicol. Environ. Saf.* **2017**, *141*, 139–147. [[CrossRef](#)]
42. Luo, C.W.; Jiang, J.; Ma, J.; Pang, S.Y.; Liu, Y.Z.; Song, Y.; Guan, C.T.; Li, J.; Jin, Y.X.; Wu, D.J. Oxidation of the odorous compound 2,4,6-trichloroanisole by UV activated persulfate: Kinetics, products, and pathways. *Water Res.* **2016**, *96*, 12–21. [[CrossRef](#)] [[PubMed](#)]

43. Qin, W.L.; Lin, Z.; Dong, H.Y.; Yuan, X.J.; Qiang, Z.M.; Liu, S.; Xia, D.S. Kinetic and mechanistic insights into the abatement of clofibric acid by integrated UV/ozone/peroxydisulfate process: A modeling and theoretical study. *Water Res.* **2020**, *186*, 116336. [[CrossRef](#)] [[PubMed](#)]
44. Fang, J.Y.; Fu, Y.; Shang, C. The roles of reactive species in micropollutant degradation in the UV/free chlorine system. *Environ. Sci. Technol.* **2014**, *48*, 1859–1868. [[CrossRef](#)] [[PubMed](#)]
45. Lu, J.H.; Dong, W.; Ji, Y.F.; Kong, D.Y.; Huang, Q.G. Natural organic matter exposed to sulfate radicals increases its potential to form halogenated disinfection byproducts. *Environ. Sci. Technol.* **2016**, *50*, 5060–5067. [[CrossRef](#)]
46. Wu, Z.H.; Chen, C.Y.; Zhu, B.Z.; Huang, C.H.; An, T.C.; Meng, F.A.; Fang, J.Y. Reactive nitrogen species are also involved in the transformation of micropollutants by the UV/Monochloramine process. *Environ. Sci. Technol.* **2019**, *53*, 11142–11152. [[CrossRef](#)] [[PubMed](#)]
47. Wang, Y.R.; Chu, W. Degradation of a xanthene dye by Fe(II)-mediated activation of oxone process. *J. Hazard. Mater.* **2011**, *186*, 1455–1461. [[CrossRef](#)]
48. Jaafarzadeh, N.; Ghanbari, F.; Zahedi, A. Coupling electrooxidation and oxone for degradation of 2,4-Dichlorophenoxyacetic acid (2,4-D) from aqueous solutions. *J. Water Process Eng.* **2018**, *22*, 203–209. [[CrossRef](#)]
49. Wang, F.G.; Wang, W.J.; Yuan, S.J.; Wang, W.; Hu, Z.H. Comparison of UV/H₂O₂ and UV/PS processes for the degradation of thiamphenicol in aqueous solution. *J. Photoch. Photobio. A* **2017**, *348*, 79–88. [[CrossRef](#)]
50. Zhou, Z.; Liu, X.T.; Sun, K.; Lin, C.Y.; Ma, J.; He, M.C.; Ouyang, W. Persulfate-based advanced oxidation processes (AOPs) for organic-contaminated soil remediation: A review. *Chem. Eng. J.* **2019**, *372*, 836–851. [[CrossRef](#)]
51. Lu, T.; Chen, Q. Realization of conceptual density functional theory and information-theoretic approach in Multiwfn program. *Concept. Density Funct. Theory* **2022**, *2*, 631–647.
52. Guo, H.G.; Ke, T.L.; Gao, N.Y.; Liu, Y.; Cheng, X. Enhanced degradation of aqueous norfloxacin and enrofloxacin by UV-activated persulfate: Kinetics, pathways and deactivation. *Chem. Eng. J.* **2017**, *316*, 471–480. [[CrossRef](#)]
53. Waclawek, S.; Lutze, H.V.; Grübel, K.; Padil, V.V.T.; Černík, M.; Dionysiou, D.D. Chemistry of persulfates in water and wastewater treatment: A review. *Chem. Eng. J.* **2017**, *330*, 44–62. [[CrossRef](#)]
54. An, T.C.; An, J.B.; Gao, Y.P.; Li, G.Y.; Fang, H.S.; Song, W.H. Photocatalytic degradation and mineralization mechanism and toxicity assessment of antiviral drug acyclovir: Experimental and theoretical studies. *Appl. Catal. B Environ.* **2015**, *164*, 279–287. [[CrossRef](#)]
55. Miao, D.; Peng, J.B.; Zhou, X.H.; Qian, L.; Wang, M.J.; Zhai, L.; Gao, S.X. Oxidative degradation of atenolol by heat-activated persulfate: Kinetics, degradation pathways and distribution of transformation intermediates. *Chemosphere* **2018**, *207*, 174–182. [[CrossRef](#)]
56. Li, M.K.; Qiang, Z.M.; Bolton, J.R.; Qu, J.H.; Li, W.T. A mini-fluidic UV photoreaction system for bench-scale photochemical studies. *Environ. Sci. Technol. Lett.* **2015**, *2*, 297–301. [[CrossRef](#)]
57. Scholes, M.L.; Schuchmann, M.N.; Sonntag, C.V. Enhancement of radiation-induced base release from nucleosides in alkaline solution: Essential role of the O^{•−} radical. *Int. J. Radiat. Biol.* **1992**, *61*, 443–449. [[CrossRef](#)]
58. Yang, Y.; Pignatello, J.J.; Ma, J.; Mitch, W.A. Effect of matrix components on UV/H₂O₂ and UV/S₂O₈^{2−} advanced oxidation processes for trace organic degradation in reverse osmosis brines from municipal wastewater reuse facilities. *Water Res.* **2016**, *89*, 192–200. [[CrossRef](#)]
59. Grebel, J.E.; Pignatello, J.J.; Mitch, W.A. Effect of halide ions and carbonates on organic contaminant degradation by hydroxyl radical-based advanced oxidation processes in saline waters. *Environ. Sci. Technol.* **2010**, *44*, 6822–6828. [[CrossRef](#)]
60. Yu, X.Y.; Bao, Z.C.; Barker, J.R. Free radical reactions involving Cl[•], Cl₂^{•−}, and SO₄^{•−} in the 248 nm Photolysis of Aqueous Solutions Containing S₂O₈^{2−} and Cl[−]. *J. Phys. Chem.* **2004**, *108*, 295–308. [[CrossRef](#)]
61. Peyton, G.R. The free-radical chemistry of persulfate-based total organic carbon analyzers. *Mar. Chem.* **1993**, *41*, 91–103. [[CrossRef](#)]
62. Klaning, U.K. Laser flash photolysis of HClO, ClO[−], HBrO, and BrO[−] in aqueous solution. Reactions of Cl[−] and Br[−] atoms. *Ber. Bunsenges. Phys. Chem.* **1985**, *89*, 243–245. [[CrossRef](#)]
63. Zehavi, D.; Rabani, J. Oxidation of aqueous bromide ions by hydroxyl radicals. Pulse radiolytic investigation. *J. Phys. Chem.* **1972**, *3*, 76. [[CrossRef](#)]
64. Lin, M.Z.; Archirel, P.; Van-Oanh, N.T.; Muroya, Y.; Fu, H.; Yan, Y.; Nagaishi, R.; Kumagai, Y.; Katsumura, Y.; Mostafavi, M. Temperature dependent absorption spectra of Br[−], Br₂^{•−}, and Br₃[−] in aqueous solutions. *J. Phys. Chem. A* **2011**, *115*, 4241–4247. [[CrossRef](#)] [[PubMed](#)]
65. Wagner, I.; Strehlow, H. On the flash-photolysis of bromide ions in aqueous-solutions. *Ber. Bunsenges. Phys. Chem.* **1987**, *91*, 1317–1321. [[CrossRef](#)]
66. Gunten, U.V.; Oliveras, Y. Advanced oxidation of bromide-containing waters: Bromate formation mechanisms. *Environ. Sci. Technol.* **1998**, *32*, 63–70. [[CrossRef](#)]
67. Matthew, B.M.; Anastasio, C. A chemical probe technique for the determination of reactive halogen species in aqueous solution Part 1-bromide solutions. *Atmos. Chem. Phys.* **2006**, *6*, 2423–2437. [[CrossRef](#)]
68. Neta, P.; Madhavan, V.; Zemel, H.; Fessenden, R.W. Rate constants and mechanisms of reaction of SO₄^{•−}, with aromatic compounds. *J. Am. Chem. Soc.* **1977**, *5*, 163–164. [[CrossRef](#)]
69. Sutton, H.C.; Downes, M.T. Reactions of the HO₂ radical in aqueous solution with bromine and related compounds. *J. Chem. Soc. Faraday Trans 1 Phys. Chem. Condens. Phases* **1972**, *68*, 1498–1507. [[CrossRef](#)]

70. Heeb, M.B.; Criquet, J.; Zimmermann-Steffens, S.G.; Gunten, U.V. Oxidative treatment of bromide-containing waters: Formation of bromine and its reactions with inorganic and organic compounds—A critical review. *Water Res.* **2014**, *48*, 15–42. [[CrossRef](#)]
71. Beckwith, R.C.; Wang, T.X.; Margerum, D.W. Equilibrium and kinetics of bromine hydrolysis. *Inorg. Chem.* **1996**, *35*, 995–1000. [[CrossRef](#)] [[PubMed](#)]
72. Liu, Y.Z.; Yang, Y.; Pang, S.Y.; Zhang, L.Q.; Ma, J.; Luo, C.W.; Guan, C.T.; Jiang, J. Mechanistic insight into suppression of bromate formation by dissolved organic matters in sulfate radical-based advanced oxidation processes. *Chem. Eng. J.* **2018**, *333*, 200–205. [[CrossRef](#)]
73. Schwarz, H.A.; Bielski, B.H.J. Reactions of hydroperoxo and superoxide with iodine and bromine and the iodide (I_2^-) and iodine atom reduction potentials. *J. Phys. Chem.* **1986**, *90*, 1445–1448. [[CrossRef](#)]
74. Buxton, G.V.; Dainton, F.S. The radiolysis of aqueous solutions of oxybromine compounds; the spectra and reactions of BrO and BrO₂. *Math. Phys. Sci.* **1968**, *304*, 427–439.